Advanced Powder Technology 26 (2015) 224–235

Contents lists available at ScienceDirect

Advanced Powder Technology

journal homepage: www.elsevier.com/locate/apt

Original Research Paper

Effects of nanoparticles diameter and concentration on natural convection of the Al_2O_3–water nanofluids considering variable thermal conductivity around a vertical cone in porous media

M. Ghalambaz [a,*], A. Behseresht [b], J. Behseresht [c], A. Chamkha [d]

[a] Department of Mechanical Engineering, Dezful Branch, Islamic Azad University, Dezful, Iran
[b] Department of Mechanical Engineering, Shahid Chamran University of Ahvaz, Ahvaz, Iran
[c] Department of Petroleum and Geosystems Engineering, University of Texas at Austin, Houston 78712, TX, United States
[d] Manufacturing Engineering Department, The Public Authority for Applied Education and Training, Shuwaikh 70654, Kuwait

ARTICLE INFO

Article history:
Received 30 July 2014
Received in revised form 22 September 2014
Accepted 1 October 2014
Available online 17 October 2014

Keywords:
Nanofluid
Variable viscosity
Variable thermal conductivity
Drift-flux model
Homogeneous model

ABSTRACT

The effects of nanoparticles diameter and concentration on natural convection heat transfer of a nanofluid around a vertical cone embedded in a Darcy porous medium is theoretically investigated utilizing the drift-flux model. The thermal conductivity and the viscosity of the nanofluid are assumed as simultaneous functions of temperature and local volume fraction of nanoparticles using experimental correlations. In addition, the flux of nanoparticles on the surface of the cone is assumed to be zero. An efficient mathematical approach with a self-similar solution is utilized to theoretically analyze the boundary layer heat and mass transfer of an Al_2O_3–water nanofluid. The reduced system of ordinary differential equations are general and can be solved for any arbitrary functions of thermal conductivity and viscosity. The analysis of the nanofluid natural convection flow is accomplished for two cases of (i) $T_w > T_\infty$ and (ii) $T_w < T_\infty$. The results show that using nanoparticles would not (would) enhance the heat transfer from the cone for the case of a cone with a hot surface (cold surface). A decrease in the size of nanoparticles or an increase in the volume fraction of nanoparticles causes a decline in the heat transfer rate from the cone when the cone surface is hot. Finally, a comparison between the non-homogenous model (drift-flux model) and the homogenous model of nanofluids is performed. The results demonstrate that the drift-flux model tends to the homogeneous model as the size and volume fraction of nanoparticles increase.

1. Introduction

Natural convection flow and heat transfer over embedded bodies in porous media has various engineering applications such as thermal energy storage, groundwater systems, flow through filtering media, and crude oil extraction [1]. Such versatile applications have attracted extensive research on natural convection phenomena over embedded bodies within porous media.

Nanofluids are widely used in various thermal systems to boost the heat transfer rate and the thermal efficiency. Nanofluids have been employed in different fields of thermal engineering such as heat exchangers, nuclear reactors, and cooling of electronic devices [2]. Utilizing nanofluids as the working fluid may enhance the heat transfer because of the enhancement in the thermal conductivity. However, other thermo-physical properties also may affect the enhancement of heat transfer of nanofluids. Some of these factors are the thermal conductivity, viscosity, density, heat capacity, dispersion and amorphous movement of nanoparticles, Brownian motion, and thermophoresis effects.

There are two known models for theoretical study of convective heat transfer of nanofluids: (i) homogeneous models and (ii) non-homogeneous models. In the homogeneous models, the nanofluid is uniform with no slip between the base fluid and nanoparticles. In the non-homogeneous models, the slip between nanoparticles and the base fluid is accounted for, and hence, the nanofluid would not be a uniform mixture of nanoparticles with a base fluid. Many researchers believe that the migration of nanoparticles within the base fluid is the significant reason behind the heat transfer enhancement of nanofluids. The migration of nanoparticles in the base fluid would transfer energy in the base fluid. Using scale analysis, Buongiorno [3] discussed seven possible mechanisms for drift flux of particles during convection of nanofluids. These are inertia, Brownian diffusion, thermophoresis, diffusion phoresis, Magnus effect, fluid

* Corresponding author. Tel.: +98 641 6260601.
E-mail addresses: m.ghalambaz@iaud.ac.ir, m.ghalambaz@gmail.com (M. Ghalambaz), behseresht.ali@gmail.com (A. Behseresht), jbehseresht@utexas.edu (J. Behseresht), achamkha@yahoo.com (A. Chamkha).

http://dx.doi.org/10.1016/j.apt.2014.10.001
0921-8831/

Nomenclature

C	a constant
Cp	specific heat (J/kg K)
D_B	Brownian diffusion coefficient (m^2/s)
d_p	diameter of nanoparticle (m)
D_T	thermophoretic diffusion coefficient (m^2/s)
f	rescaled nanoparticles volume fraction, nanoparticles concentration
g	gravitational acceleration vector (m/s^2)
h	convective heat transfer coefficient
k	thermal conductivity (W/m K)
k_B	Boltzmann's constant (1.3807×10^{-23} J/K)
Le	Lewis number
Nb	Brownian motion parameter
Nr	buoyancy ratio
Nt	thermophoresis parameter
Nu	Nusselt number
P	pressure (Pa)
q_w	surface heat flux
Ra_x	local Rayleigh number
r	local radius of the cone
S	dimensionless stream function
T	temperature (K)
u, v	Darcy velocity components (m/s)
(x, y)	Cartesian coordinates

Greek symbols

(ρc)	heat capacity (J/m^3 K)
μ	viscosity (Pa s)
α	thermal diffusivity (m^2/s)
β	volumetric expansion coefficient of fluid (1/K)
ε	porosity
γ	cone half-angle
η	dimensionless distance
θ	dimensionless temperature
κ	permeability of porous medium (m^2)
ρ	fluid density (kg/m^3)
ϕ	nanoparticles volume fraction
ψ	stream function

Subscripts

∞	ambient
eff	effective property between porous medium and nanofluid
f	the base fluid
nf	nanofluid
p	nanoparticles
s	porous medium
w	wall

drainage, and gravity. However, only the thermophoresis and the Brownian diffusion effects were found to be important [3,4].

Nield and Kuznetsov [5] have extended the work of Buongiorno [3] to the heat transfer of nanofluids in porous media. They have analyzed the natural convection flow of nanofluids over an isothermal flat plate taking into account the Brownian motion and thermophoresis effects. They [5] found that the reduced Nusselt number is a decreasing function of the Brownian motion and thermophoresis parameters. Yih [6] numerically explored the effect of uniform lateral mass flux on natural convection around a cone embedded in a saturated porous medium using a similarity solution. Recently, Rashad et al. [7] have extended work of Yih [6] to the natural convection flow of nanofluids. They [7] have analyzed the heat transfer associated via migration of nanoparticles. They found that as the thermophoresis, Brownian motion and buoyancy ratio parameters increase, the reduced Nusselt number decreases. Natural convective boundary layer flow of a nanofluid over a horizontal plate embedded in a saturated porous medium has been examined by Gorla and Chamkha [8]. Chamkha et al. [9] presented a non-similar solution for natural convective boundary layer flow over a sphere embedded in a nanofluid-saturated porous medium. Rana et al. [10] analyzed the boundary layer heat transfer of nanofluids over an inclined plate embedded in a porous medium. In a recent work, Noghrehabadi et al. [11] have investigated non-Darcy flow and natural convection of nanofluids over a vertical cone embedded in a porous medium. They [11] have reported that the reduced Nusselt number decreases with an increase in the non-Darcy parameter. Noghrehabadi et al. [12] have studied natural convection heat and mass transfer of nanofluids over a vertical plate embedded in a porous medium by applying surface heat and nanoparticle fluxes as boundary conditions. Furthermore, Noghrehabadi and Behseresht [13] analyzed the flow and heat transfer of nanofluid over a cone placed in porous media. Considering the viscosity and thermal conductivity of nanofluids as a linear function of local volume fraction of nanoparticles, they studied the effect of variable properties on the flow and heat transfer of a nanofluid. The important outcome has shown that the reduced Nusselt number would increase with increase of viscosity parameter and decrease with an increase of thermal conductivity parameter [13]. In addition, Gorla et al. [14] have recently studied the nanofluid flow boundary layer for the natural convection over a non-dimensional vertical cone in a porous medium.

In the mentioned works [7–12], the effects of temperature and local volume concentration of nanoparticles on the thermal conductivity and viscosity of nanofluids were neglected. However, experiments demonstrate that the thermal conductivity and the dynamic viscosity of nanofluids strongly depend on both of the volume fraction of nanoparticles and temperature [4,15,16]. Indeed, although the effect of temperature on the thermal conductivity and the dynamic viscosity of conventional pure fluids can be neglected for small temperature differences, these effects cannot be neglected for nanofluids owing to the presence of nanoparticles [15]. Therefore, in the present study, experimental correlations as simultaneous functions of temperature and local volume fraction of nanoparticles are adopted to include the local effect of temperature and volume fraction of nanoparticles on the thermal conductivity and the dynamic viscosity of an Al_2O_3–water nanofluid.

Previous studies [7–12] have approximated the volume fraction of nanoparticles on the surface to be constant, but this constant is unknown and no effort was made to calculate it. Accomplishing a case study, however, requires the exact value of nanoparticles volume fraction on the surface. Furthermore, an approximation of constant value of nanoparticles volume fraction on the surface generally implies a non-zero value of particles mass flux at the surface. This is an unrealistic assumption since the particles cannot cross the surface. Hence, assuming a zero particle mass flux through the surface as a boundary condition makes a more physical sense.

In this paper, a zero particle flux through the cone surface is utilized as a new auxiliary boundary condition. Furthermore, using similarity variables, the governing partial differential equations are converted into a set of ordinary differential equations. A case study for an Al_2O_3–water nanofluid, as a typical nanofluid, is conducted. The experimental correlations in the literature are then used to evaluate the local values of the dynamic viscosity and the thermal conductivity. Moreover, the nanoparticles volume fraction at the cone surface is also evaluated.

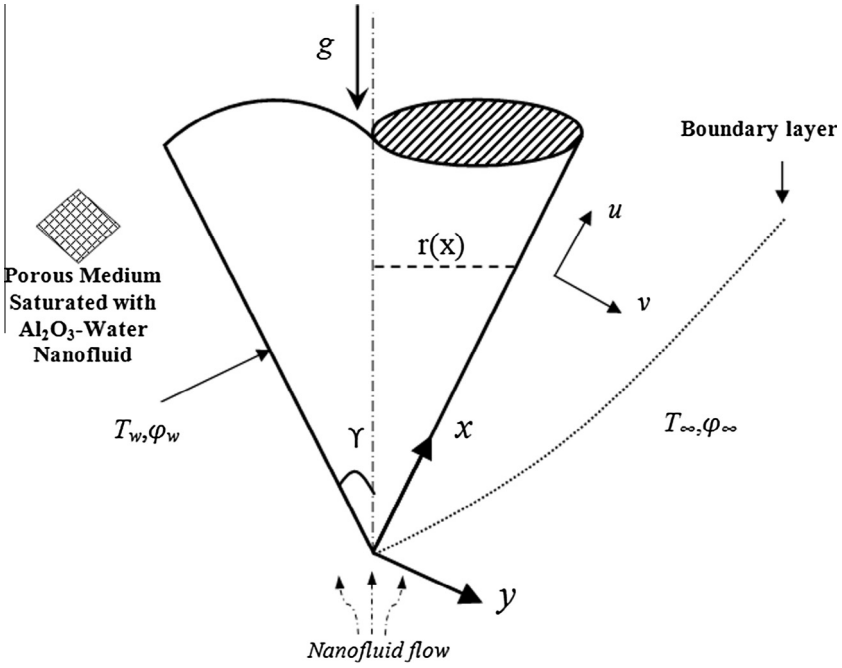

Fig. 1. Physical model and coordinate system.

2. Mathematical analysis

Fig. 1 illustrates a two-dimensional, incompressible, laminar and steady natural convection boundary layer flow of a nanofluid around a vertical cone within a saturated porous medium. The coordinate system is chosen such that the x-axis is coincident with the flow direction over the cone surface. The temperature of the cone surface can be higher or lower than the ambient temperature.

As mentioned earlier, the nanoparticles within the base fluid are subject to forces including thermophoresis and Brownian motion forces. The thermophoresis acts against the temperature gradient, meaning that the particles tend to move from hot regions to cold ones [3]. The Brownian motion tends to move the particles from high concentration areas to low concentration areas. Considering the case in which the temperature at the cone surface is higher than the ambient temperature, the nanoparticles are expected to move away from the surface of cone. In contrast, the Brownian motion force tends to make the concentration of nanoparticles uniform. This would create a concentration boundary layer of nanoparticles over the surface of the cone. For the case, in which the temperature at the surface of the cone is lower than that of the ambient temperature, the temperature gradient has a tendency to move nanoparticles into the surface due to the thermophoresis effect. In contrast, the Brownian motion effect tends to uniform the nanoparticles. Hence, in this case, there is also a concentration boundary layer over the cone. However, the concentration of nanoparticles at the surface of the cone is higher than that of the ambient temperature.

There are three distinct boundary layers namely: (i) hydrodynamic, (ii) thermal and (iii) nanoparticles concentration over the cone, however, only one of the boundary layer is symbolically plotted in Fig. 1. It is assumed that the cone surface is isothermal, and the nanoparticle volume fraction (ϕ) at the cone surface ($y = 0$) is ϕ_w. The constant value of ϕ_w, however, is unknown and needs to be evaluated later. T_∞ and ϕ_∞ denote the ambient temperature and nanoparticles volume fraction, respectively. The flow within the porous medium with porosity ε and permeability κ is assumed to be a Darcy flow. The porous medium is also assumed homogeneous, and in local thermal equilibrium with the nanofluid.

Following the reference work of Buongiorno [3] and by employing the Oberbeck–Boussinesq approximation and applying the standard boundary layer approximations [11,17], the following four equations embody basic steady-state balance laws of total mass, momentum, thermal energy, and nanoparticles for nanofluids in the Cartesian coordinate system of x and y as follows:

$$\frac{\partial(ru)}{\partial x}+\frac{\partial(rv)}{\partial y}=0 \tag{1}$$

$$\begin{cases} \frac{\partial p}{\partial y}=0, \\ \mu_{nf,\infty}\left(\frac{\mu(\phi,T)}{\mu_{nf,\infty}}\right)\frac{1}{\kappa}u=-\frac{\partial p}{\partial x}+g\Big[(1-\phi_\infty)\beta\rho_{f_\infty}(T-T_\infty) \\ \qquad\qquad -\left(\rho_P-\rho_{f_\infty}\right)(\phi-\phi_\infty)\Big]\cos\gamma \end{cases} \tag{2}$$

$$(\rho c)_{nf}\left(u\frac{\partial T}{\partial x}+v\frac{\partial T}{\partial y}\right)=k_{eff,nf,\infty}\frac{\partial}{\partial y}\left(\frac{k_{eff,nf}(\phi,T)}{k_{eff,nf,\infty}}\frac{\partial T}{\partial y}\right) +\varepsilon(\rho c)_p\left[D_B\frac{\partial\varphi}{\partial y}\frac{\partial T}{\partial y}+\frac{D_T}{T_\infty}\left(\frac{\partial T}{\partial y}\right)^2\right] \tag{3}$$

$$\frac{1}{\varepsilon}\left[u\frac{\partial\phi}{\partial x}+v\frac{\partial\phi}{\partial y}\right]=D_B\frac{\partial^2\phi}{\partial y^2}+\left(\frac{D_T}{T_\infty}\right)\frac{\partial^2 T}{\partial y^2} \tag{4}$$

Based on the problem description, the boundary conditions at the cone surface are:

$$v=0,\quad T=T_w,\quad \phi=\phi_w,\quad \text{at } y=0 \tag{5}$$

The boundary conditions far away from the cone surface (ambient space) are:

$$u\to u_\infty,\quad T\to T_\infty,\quad \phi\to\phi_\infty,\quad \text{at } y\to\infty \tag{6}$$

where the subscripts ∞ and w indicate the properties outside the boundary layer and at the cone surface, respectively. The subscripts P, nf and f denote properties corresponding to the nanoparticles, nanofluid and the base fluid, respectively. The subscript *eff* denotes the effective properties of the porous medium and the nanofluid. Here, $k_{eff,nf}$ is the effective thermal conductivity of the porous medium and the nanofluid.

If the thermal boundary layer is thin, r can be approximated by the local radius of the cone [11]. The set of equations introduced in Eq. (2), are simplified using cross-differentiation, and the

continuity equation, Eq. (1), will also be satisfied by introducing a stream function, (ψ):

$$u = \frac{1}{r}\frac{\partial \psi}{\partial y}, \quad v = -\frac{1}{r}\frac{\partial \psi}{\partial x} \tag{7}$$

Here, the local Rayleigh number, Ra_x, and the similarity variable, η, are defined by:

$$Ra_x = \frac{(1-\phi_\infty)\rho_{f\infty}\beta\kappa g\cos\gamma(T_w - T_\infty)x}{\mu_{nf,\infty}\alpha_{eff,nf,\infty}} \tag{8}$$

$$\eta = \frac{y}{x}Ra_x^{\frac{1}{2}} \tag{9}$$

The dimensionless similarity quantities S, θ, and f are introduced as:

$$S = \frac{\psi}{\alpha_{eff,nf,\infty}\cdot r\cdot Ra_x^{\frac{1}{2}}}, \quad f = \frac{\phi-\phi_\infty}{\phi_w-\phi_\infty}, \quad \theta = \frac{T-T_\infty}{T_w-T_\infty} \tag{10}$$

The local radius of the cone is related to the x coordinate by,

$$r = x\sin\gamma \tag{11}$$

Applying Eqs. (9) and (10) onto Eqs. (1)–(4), the following three ordinary differential equations are obtained (see Appendix A):

$$\left(\frac{\mu_{nf}(f,\theta)}{\mu_{nf,\infty}}\right)S'' + \left(\frac{\mu_{nf}(f,\theta)}{\mu_{nf,\infty}}\right)'S' - \theta' + \Delta\phi\cdot Nr\cdot f' = 0 \tag{12}$$

$$\frac{k_{eff,nf}(f,\theta)}{k_{eff,nf,\infty}}\theta'' + \left(\frac{k_{eff,nf}(f,\theta)}{k_{eff,nf,\infty}}\right)'\theta' + \frac{3}{2}S\theta' + \Delta\phi\cdot Nb\cdot f'\theta' + Nt\cdot\theta'^2 = 0 \tag{13}$$

$$f'' + \frac{3}{2}\cdot Le\cdot S\cdot f' + \frac{Nt}{\Delta\phi\cdot Nb}\theta'' = 0 \tag{14}$$

subject to the following dimensionless boundary conditions:

$$\text{at the cone surface}: \ \eta = 0: \ S = 0, \quad \theta = 1, \quad f = 1 \tag{15a}$$

$$\text{and far away from the cone}: \ \eta\to\infty: \ S' = 0, \quad \theta = 0, \quad f = 0 \tag{15b}$$

where the non-dimensional physical parameters; buoyancy ratio, Brownian motion, thermophoresis and the Lewis number are, respectively defined as follows:

$$Nr = \frac{\left(\rho_p - \rho_{f\infty}\right)}{\rho_{f\infty}\beta(T_w-T_\infty)(1-\phi_\infty)} \tag{16a}$$

$$Nb = \frac{\varepsilon(\rho c)_p D_B}{(\rho c)_f \alpha_{eff,nf,\infty}} \tag{16b}$$

$$Nt = \frac{\varepsilon(\rho c)_p D_T(T_w-T_\infty)}{(\rho c)_f \alpha_{eff,nf,\infty}T_\infty} \tag{16c}$$

$$Le = \frac{\alpha_{eff,nf,\infty}}{\varepsilon D_B} \tag{16d}$$

where $\Delta T = T_w - T_\infty$ and $\Delta\phi = \phi_w - \phi_\infty$. Here, ϕ_w and consequently $\Delta\phi$ are unknown parameters as yet. It is interesting that integrating Eq. (12) yields:

$$\left(\frac{\mu_{nf}(f,\theta)}{\mu_{nf,\infty}}\right)S' - \theta + \Delta\phi\cdot Nr\cdot f = C \tag{17a}$$

where C is a constant which originates from the integration. Using the boundary conditions of Eq. (15b), C turns out to be zero. Solving Eq. (17a) with the boundary conditions Eq. (15a), reveals that the non-dimensional surface velocity at the cone surface is a function of the boundary ratio parameter (Nr) and the concentration difference ($\Delta\phi$):

$$S'(0) = 1 - \Delta\phi\cdot Nr \tag{17b}$$

The local Nusselt number (Nu_x) is defined as:

$$Nu_x = \frac{h\cdot x}{k_{eff,nf,\infty}} = \frac{q_w x}{k_{eff,nf,\infty}(T_w-T_\infty)} \tag{18}$$

where q_w is the surface heat flux.

Using the similarity variables, Eq. (10), the reduced Nusselt number (Nu_r) is obtained as follows:

$$Nu_r = Nu_x Ra_x^{-\frac{1}{2}} = -\frac{k_{eff,nf,w}}{k_{eff,nf,\infty}}\theta'(0) \tag{19}$$

It was assumed that the concentration at the cone surface is ϕ_w, and thus, the value $\Delta\phi$ is unknown. This raises the necessity of a new boundary condition in order to determine the value of $\Delta\phi$. The surface of the cone is assumed impermeable, and thus, the mass flux from the cone surface can be set to zero as:

$$D_B\frac{\partial\phi}{\partial y} + \frac{D_T}{T_\infty}\frac{\partial T}{\partial y} = 0 \tag{20}$$

As the concentration difference increases (the increase of the magnitude of $|\Delta\phi|$), the Brownian motion force at the surface gets stronger. When the Brownian force is equal to the thermophoresis force, the nanoparticles would not tend to cross the surface. Indeed, for this nanofluid phenomenon, we have a situation in which the flux of nanoparticles at the surface is zero and the concentration of nanoparticles at the surface is also constant. The reason for such an effect is the fact that the concentration of nanoparticles is adjusted at the surface by the boundary layer characteristics (and not by the external applied force). Using the similarity variables, Eq. (20) is transformed to the following auxiliary boundary condition:

$$f'(0) + \frac{Nt}{\Delta\phi\cdot Nb}\theta'(0) = 0 \tag{21}$$

Therefore, the reduced Sherwood number, Eq. (21), shows the mass transfer from the surface is identically zero.

In practice, the enhancement of heat transfer due to the presence of nanoparticles in the base fluid is of interest. Therefore, an enhancement ratio parameter is introduced as:

$$\frac{h_{nf}}{h_f} = \frac{k_{eff,nf,w}\theta'_{nf}(0)Ra_{nf\ x}^{\frac{1}{2}}}{k_{eff\,f,w}\theta'_{bf}(0)Ra_{bf\ x}^{\frac{1}{2}}} \tag{22}$$

which represents the ratio of convective heat transfer of nanofluids to the convective heat transfer of the base fluid.

The ratio of the heat transfer coefficient evaluated using a drift-flux model (dynamic) to the homogeneous model (static) shows the effect of concentration gradient on the heat transfer. Therefore, the enhancement ratio of the dynamic model to the static model is introduced as follows:

$$\frac{h_{Dynamic}}{h_{Static}} = \frac{k_{w,Dynamic}\theta'_{nf,Dynamic}(0)}{k_{w,Static}\theta'_{bf,Static}(0)} \tag{23}$$

In order to calculate the thermo-physical properties of the nanofluid and their derivatives in Eqs. (12) and (13) and finally solve the three coupled Eqs. (12)–(14), the dynamic viscosity and the effective thermal conductivity of the nanofluid and the porous medium as functions of the non-dimensional temperature and the non-dimensional concentration of nanoparticles are required. Recently, Khanafer and Vafai [15] have reviewed the experimental

works on the thermo-physical properties of nanofluids. They have proposed correlations for the dynamic viscosity and the thermal conductivity of Al_2O_3–water nanofluids as function of the temperature, volume fraction of nanoparticles and the size of nanoparticles using curve fitting of the available experimental data. The correlations for the dynamic viscosity and the thermal conductivity of Al_2O_3–water nanofluids, reported by Khanafer and Vafai [15], are as follows:

$$\mu_{nf}(f,\theta)=\begin{pmatrix}-0.4491+\frac{28.837}{T}+0.574\phi\times10^2-0.1634\phi^2\times10^4+23.053\frac{\phi^2}{T^2}\times10^4\\+0.0132\phi^3\times10^6-2354.735\frac{\phi}{T^3}\times10^2+23.498\frac{\phi^2}{d_p^2}\times10^4-3.0185\frac{\phi^3}{d_p^2}\times10^6\end{pmatrix}\times10^{-3} \quad (24)$$

$$\text{for}: \ 0.01\leqslant\phi\leqslant0.09, \quad 20\leqslant T(^\circ\text{C})\leqslant70, \quad 13\ \text{nm}\leqslant d_p\leqslant131\ \text{nm}$$

$$k_{nf}=k_f\begin{pmatrix}0.9843+0.398\left(\phi\times10^2\right)^{0.7383}d_p^{-0.2246}\left(\frac{\mu_{nf}}{\mu_f}\right)^{0.0235}\\-3.9517\frac{\phi}{T}\times10^2+34.034\frac{\phi^2}{T^2}\times10^4+32.509\frac{\phi}{T^2}\times10^2\end{pmatrix}$$

$$\text{for}: \ 0.0\leqslant\phi\leqslant0.10, \quad 20\leqslant T(^\circ\text{C})\leqslant70, \quad 11\ \text{nm}\leqslant d_p\leqslant150\ \text{nm} \quad (25)$$

where

$$\mu_f=2.414\times10^{-5}\times10^{\frac{247.8}{T+133}}, \quad T(^\circ\text{C}) \quad (26)$$

The correlations of the dynamic viscosity and the thermal conductivity can be written as a functions of f and θ using $T=(T_w-T_\infty)\theta+T_\infty$ and $\phi=(\phi_w-\phi_\infty)f+\phi_\infty$. The effective thermal conductivity of the porous medium and the nanofluid is evaluated using the weighted geometric mean of k_s and k_{nf}, defined as [18]:

$$k_{eff,nf}=k_s^{1-\varepsilon}k_{nf}^{\varepsilon} \quad (27)$$

where k_s, k_{nf} and ε are the thermal conductivity of the porous medium, the thermal conductivity of the nanofluid, and the porosity of the porous medium, respectively. This relation provides a good estimate so long as k_s and k_{nf} are not too different from each other. Moreover, the terms of $d\mu(f,\theta)/d\eta$ and $dk_{eff}(f,\theta)/d\eta$ and other thermo-physical relations are reported in the Appendix B.

3. Numerical method of solution

The system of Eqs. (12)–(14) with the boundary conditions (15) and (21) is numerically solved using a finite-difference solver [17]. A collocation method with automatic grid adaptation is utilized to control the convergence and error of the solution. The solver is the same as that in Shampine et al. [17]. A maximum relative error of 10^{-10} is used as the stopping criteria for the iterations. The concentration equation, Eq. (14), is a second order equation, containing the unknown parameter $\Delta\phi$. There are also three boundary conditions for this equation in Eqs. (15a), (15b) and (20). Therefore, the set of governing equations, involving the unknown parameter $\Delta\phi$, are solved subject to the boundary conditions simultaneously. A sensible criterion for making the numerical approach accurate is to choose an appropriate finite value of η_∞. Therefore, in order to estimate the relevant value of η_∞, the solution process has been commenced with an initial value of $\eta_\infty=5$, and then Eqs. (12)–(14) are solved subject to the boundary conditions (15) and (21). In order to check and correct the value of η_∞ until further changes in η_∞ did not lead to any changes in the values of the results, the solution process is orderly repeated. The choice of $\eta_{max}=10$ ensured that all numerical solutions approach to the asymptotic values at the free stream conditions correctly. It is worth noticing that, when the governing equations are solved, the unknown value of $\Delta\phi$ which is a part of the solution process will also be determined. As $\Delta\phi$ is determined, the concentration at the surface can simply be evaluated using the definition of $\Delta\phi$ as $\phi_w=\Delta\phi+\phi_\infty$. As seen, the value of $\Delta\phi$ and ϕ_∞ are scalar values, and hence, ϕ_w is also a scalar value, which means that the concentration of nanoparticles at the surface is a constant value, adjusted by the boundary layer characteristics (notice that $\Delta\phi$ was adjusted in the solution procedure to satisfy the boundary condition in Eq. (20)).

In order to check the accuracy of the solution, the value of Nur is compared with the reported values by Yih [6] and Cheng et al. [19]. Neglecting the effects of the nanofluid parameters, $Nb=Nt=Nr=0$, and assuming constant values of the thermo-physical properties, the present study reduces to the works of Yih [6] and Cheng et al. [19]. Excellent agreement between the present results and those of Yih [6] and Cheng et al. [19] exists as the value of $-\theta'(0)$ is calculated as 0.7686 in the work of Yih [6] and 0.7685 in the work of Cheng et al. [19] whereas in the present study, this value is computed as 0.76859.

4. Results and discussion

Recently, Behseresht et al. [20] investigated the values of nanofluid parameters (Thermophoresis, Brownian motion, Buoyancy ratio and Lewis number). They presented the practical ranges of nanofluid thermo-physical properties. In the present paper, the realistic values of nanofluid parameters obtained by Behseresht et al. [20] have been adopted. The following values are adopted for a case study when the cone surface is hot and the ambient space is cold: $T_\infty=30\ ^\circ\text{C}$, $\Delta T=20\ ^\circ\text{C}$, $d_p=30$ nm. The following values are also adopted for a case study when the cone surface is cold and the ambient space is hot: $T_\infty=50\ ^\circ\text{C}$, $\Delta T=-20\ ^\circ\text{C}$, $d_p=30$ nm. It is worth noticing that the case of a cone with a hot surface is more practical than that of a cold surface, as in most practical cases, the heat should be removed from the hot surface into the ambient space. However, there are also few cases in which there is a reaction or heat absorbing process inside the cone in which the cone should be heated from the ambient space. Hence, the main focus of the study is to analysis the cone with the hot surface. However, in some cases, a cone with a cold surface is also studied.

The porosity of the porous medium is fixed as $\varepsilon=0.5$ and the thermal conductivity of the porous medium is assumed equal to the thermal conductivity of the base fluid ($k_s\approx k_f\approx0.6065$) for convenience. The details of the thermo-physical models are given in Appendix B. The thermal conductivity of water is computed using Eq. (B.1). The thermo-physical properties of water as well as Al_2O_3 nanoparticles are assumed as shown in Table 1. In the following text, all the results are reported for the mentioned thermo-physical properties and assumptions unless otherwise stated.

In order to check the correctness of the solution, the results are compared with the results of Runge–Kutta–Fehlberg method. In

Table 1
Thermo-physical properties of base fluid [4,13], Al_2O_3 nanoparticles [13].

Physical properties	ρ (kg/m^3)	Cp	β (K^{-1})	K (W/m K)
Water	997.1	4179	21×10^{-5}	0.613
Al_2O_3 nanoparticles	3970	765	0.85×10^{-5}	40

Table 2
The non-dimensional parameters and the calculated values of $S'(0)$, $\theta'(0)$, $f'(0)$ and $\Delta\phi$ when T_∞ = 30 °C, ΔT = 20 °C, and ε = 0.5.

ϕ_∞	d_p	$S'(0)$	$\theta'(0)$	$f'(0)$	$\Delta\varphi$	Nr	Nb	Nt	Le
2%	20	1.618986	−0.76814	−123.815	−0.00091	683.615	6.51E−05	9.50E−06	11263.05
	30	1.743823	−0.76799	−154.521	−0.00109	683.615	4.40E−05	9.63E−06	16667.92
	40	1.845441	−0.76787	−181.236	−0.00124	683.615	3.33E−05	9.71E−06	22025.6
	50	1.932532	−0.76777	−205.363	−0.00136	683.615	2.68E−05	9.78E−06	27349.94
	60	2.009486	−0.76769	−227.626	−0.00148	683.615	2.24E−05	9.83E−06	32648.78
	70	2.078876	−0.76763	−248.461	−0.00158	683.615	1.93E−05	9.87E−06	37927.16
	80	2.142359	−0.76757	−268.154	−0.00167	683.615	1.70E−05	9.91E−06	43188.52
	90	2.201074	−0.76751	−286.906	−0.00176	683.615	1.51E−05	9.94E−06	48435.4
	100	2.255843	−0.76746	−304.863	−0.00184	683.615	1.37E−05	9.96E−06	53669.72
4%	20	2.071674	−0.76685	−137.996	−0.00162	660.6773	6.35E−05	1.85E−05	11598.91
	30	2.280157	−0.76648	−173.2	−0.00194	660.6773	4.33E−05	1.90E−05	17014.81
	40	2.448719	−0.76621	−203.992	−0.00219	660.6773	3.30E−05	1.92E−05	22352.1
	50	2.592532	−0.766	−231.899	−0.00241	660.6773	2.67E−05	1.95E−05	27633.34
	60	2.719186	−0.76582	−257.719	−0.0026	660.6773	2.24E−05	1.96E−05	32871.4
	70	2.8331	−0.76568	−281.934	−0.00277	660.6773	1.94E−05	1.98E−05	38074.58
	80	2.937103	−0.76555	−304.859	−0.00293	660.6773	1.70E−05	1.99E−05	43248.67
	90	3.033132	−0.76543	−326.719	−0.00308	660.6773	1.52E−05	2.00E−05	48397.88
	100	3.122577	−0.76533	−347.678	−0.00321	660.6773	1.38E−05	2.01E−05	53525.44

the case of T_∞ = 30 °C, ΔT = 20 °C, dp = 30 nm, and ε = 0.5, the non-dimensional parameters and the calculated values of $S'(0)$, $\theta'(0)$, $f'(0)$ and $\Delta\phi$, are reported in Table 2. Based on the results of this table, the governing boundary value differential Eqs. (12)–(14) can be seen as an initial-value ordinary differential equation without any unknown parameter. Therefore, according to the results of Table 2, the governing equations were solved using the Runge–Kutta–Fehlberg method with variable size steps and error control [21]. The maximum truncation error was fixed as 1×10^{-10}. The average number of required steps was about 24,000. The results of the Runge–Kutta–Fehlberg method revealed that the asymptotic boundary conditions were correctly satisfied. The results of the Runge–Kutta–Fehlberg method were found to be in excellent agreement with the results of the finite-difference method. It is worth noticing that the Lewis number for nanofluids is very small, and hence, the thickness of the concentration boundary layer is much lower than the thickness of thermal boundary layer. In addition, there is an unknown parameter, $\Delta\phi$, in the differential equations. Thus, the convergence of the present boundary value problem requires good initial guesses or the utilizing of continuation methods. Hence, the results of Table 2 can be utilized as initial guesses for future studies.

Fig. 2a and b shows the effect of the nanoparticles volume fraction and diameter on the concentration difference, ($\Delta\phi$), for two cases of a cone with a hot surface and cone with a cold surface, respectively. In these figures, three cases of nanoparticles diameters, i.e. 30, 60 and 90 nm have been adopted. As seen in Fig. 2a, the magnitude of the nanoparticles concentration difference ($\Delta\phi$) increases by increasing the nanoparticles volume fraction and nanoparticles diameter. According to the results of Table 2, as the nanoparticles size increases, the values of thermophoresis parameter, Brownian motion parameter and the temperature gradient at the cone surface remains approximately constant whereas the nanoparticles concentration gradient at the cone surface increases significantly. Therefore, considering Eq. (21), the magnitude of the concentration difference ($|\Delta\phi|$) increases as the concentration gradient of the nanoparticles at the surface of the cone increases. Moreover, it is clear that the values of $\Delta\phi$ are negative, and hence, the volume fraction of the nanoparticles in the vicinity of the cone surface is lower than the volume fraction of the nanoparticles outside the boundary layer. Indeed, the thermophoresis force moves the nanoparticles from the hot areas in the vicinity of the cone to the low temperature areas. However, it should be noticed that the concentration difference ($\Delta\phi$) is very low (about 0.33% volume fraction of nanoparticles). Fig. 2b shows that the concentration

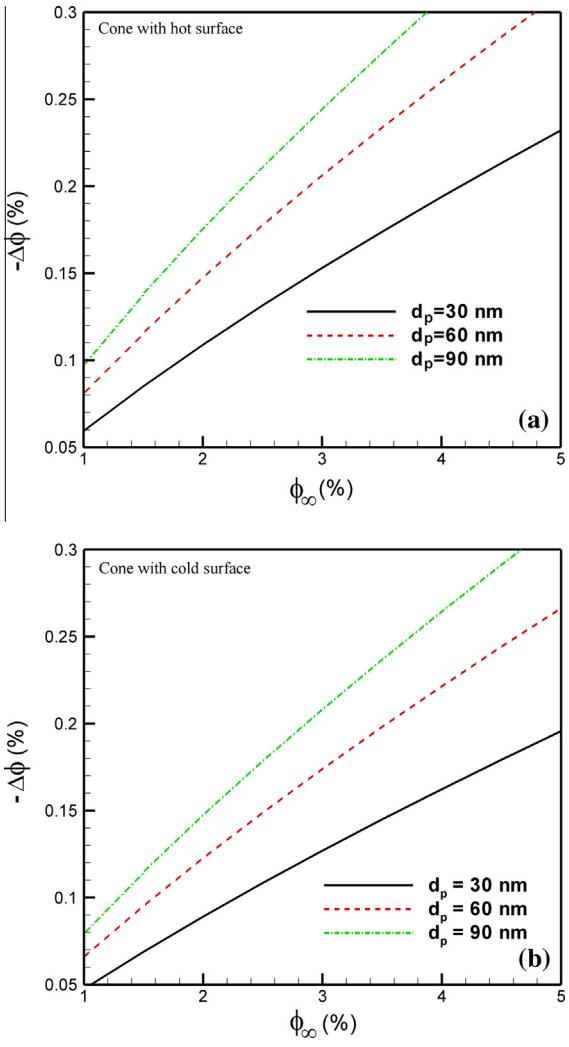

Fig. 2. The effects of nanoparticles volume fraction and diameter on the concentration difference ($\Delta\varphi$) ((a) the cone with hot surface and (b) the cone with cold surface).

difference ($\Delta\phi$) adopts positive values. The positive values of the concentration difference are because of the thermophoresis effect. The thermophoresis effect tends to collect the nanoparticles on the

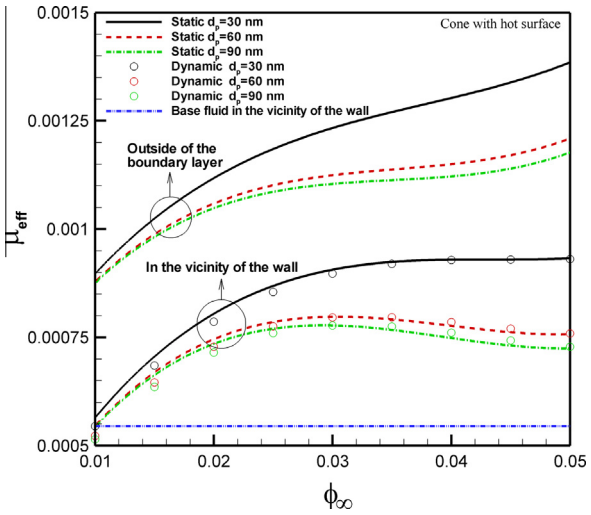

Fig. 3. The effects of nanoparticles volume fraction and diameter on the dynamic viscosity.

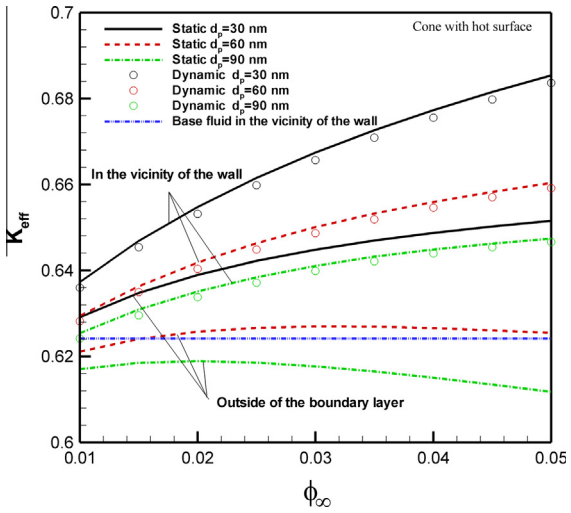

Fig. 4. The effects of nanoparticles volume fraction and diameter on the thermal conductivity.

surface, and hence, the concentration of nanoparticles at the surface is higher than that of the ambient space. A comparison between the results of Fig. 2a and b depicts that the magnitude of the concentration difference ($|\Delta\phi|$) for the case of a cone with a hot surface is smoothly higher than that of a cone with a cold surface. As the results of $\Delta\phi$ are plotted in Fig. 2 for any value of ϕ_∞, the volume fractions of nanoparticles at the surface (ϕ_w) can be easily evaluated as $\phi_w = \Delta\phi + \phi_\infty$.

The effects of the ambient volume fraction (ϕ_∞) and the nanoparticles diameter on the dynamic viscosity and the thermal conductivity of Al_2O_3–water nanofluid, evaluated using the dynamic model, and the static model as well as for the base fluid, are depicted in Figs. 3 and 4, respectively. The results are obtained for the case in which the surface of the cone is hot. In the dynamic model, the simultaneous effect of the local volume fraction of nanoparticles and the local temperature is taken into account. In the static model, the effect of local temperature is solely taken into account. In the model of pure water, only the effect of temperature is taken into account. Therefore, the properties of pure water are a straight line against the ambient volume fraction of nanoparticles. As seen, an augmentation of the nanoparticles size reduces the thermal conductivity and the dynamic viscosity of the nanofluid. In contrast, an increase in the ambient volume fraction of nanoparticles, ϕ_∞, raises the thermal conductivity and the dynamic viscosity of the nanofluid. Moreover, the dynamic viscosity of the nanofluid in the vicinity of the cone surface, where the temperature is high, is lower than the dynamic viscosity at the ambient free stream where the temperature is low. The thermal conductivity of the nanofluid near the cone surface, where the temperature is high, is higher than the thermal conductivity of the ambient free stream where the temperature is low. In Fig. 3, it is clear that as the size of nanoparticles increases, its effect on the variation of dynamic viscosity is decreased. For example, there is a large difference between the dynamic viscosity of a nanofluid with 30 nm nanoparticles and the dynamic viscosity of a nanofluid with 60 nm particles, but the difference between those of 60 nm and 90 nm is comparatively negligible. The outcomes show that the temperature and the size of nanoparticles are two important factors for the variation of the dynamic viscosity of a nanofluid. In addition, it is observed that up to a 3% nanoparticles volume fraction, the curves are significantly ascending. However, as the nanoparticles concentration increases, the ascending trend suppresses. Moreover, the dynamic viscosity and the thermal conductivity of both the dynamic and static models in the vicinity of the cone surface are compared in Figs. 3 and 4, respectively. In the static model, the nanofluid is homogenous, and thus, the concentration of nanoparticles near the cone surface is the same as the concentration of ambient free stream. Hence, in the case of the static model, the difference between the thermo-physical properties near the cone surface and the ambient free stream is solely due to the temperature difference between the cone surface and ambient free stream (ΔT). In the dynamic model, the concentration of nanoparticles near the cone surface is different from the ambient concentration ($\Delta\phi < 0$). Thus, the reason for the difference between the thermo-physical properties of the nanofluid near the cone surface and the ambient free stream is the simultaneous effects of the temperature difference (ΔT) and the nanoparticles concentration difference ($\Delta\phi$). Figs. 3 and 4 reveal that the thermo-physical properties evaluated by the static and dynamic models are almost coincident. The reason for this behavior is that the concentration difference ($\Delta\phi$) between the cone surface and the ambient free stream is very low ($\Delta\phi \approx 0.33\%$).

The Brownian motion parameter (Nb) and the Lewis number (Le) are plotted as functions of the ambient volume fraction (ϕ_∞) and the nanoparticles diameter (d_P) in Figs. 5 and 6, respectively when the surface of the cone is hot. These figures show that

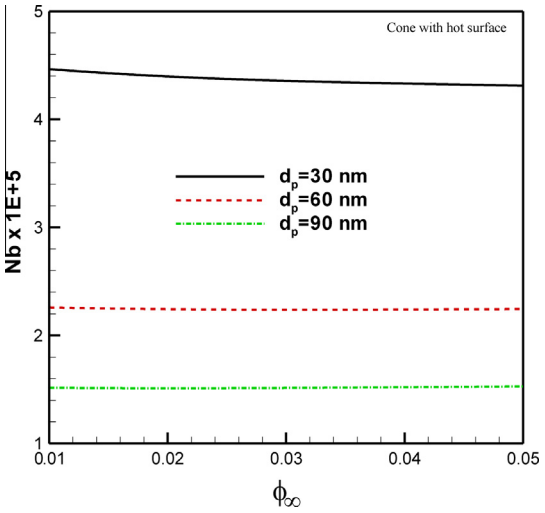

Fig. 5. The effects of nanoparticles volume fraction and diameter on the Brownian motion parameter.

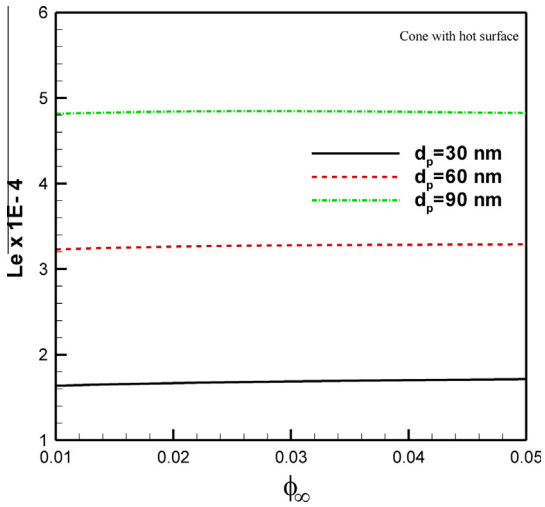

Fig. 6. The effects of nanoparticles volume fraction and diameter on the Lewis number.

increasing the nanoparticles diameter significantly decreases the Brownian motion parameter and increases the Lewis number. However, the variation of the nanoparticles volume fraction (ϕ_∞) does not significantly lead to affect *Nb* and *Le*. The Lewis number is an increasing function of the nanoparticles size. In fact, the augmentation of the size of the nanoparticles tends to reduce the thermal conductivity of the nanofluid (k_{nf}) as well as the Brownian motion coefficient (D_B). However, the decline of the Brownian motion coefficient (D_B) is much stronger than the raise of the thermal conductivity, and thus, an augmentation of the size of the nanoparticles raises the Lewis number. Fig. 5 depicts that the Brownian motion parameter for nanofluids is very small (about 10^{-5}), and Fig. 6 shows that the Lewis number is very high (about 4×10^4).

It is found that the size of nanoparticles has no significant effect on the buoyancy ratio parameter (*Nr*) and the thermophoresis parameter (*Nt*) (see Table 2). Hence, the variation of these parameters is not plotted in the figures. However, the concentration of nanoparticles significantly affects these parameters. Table 3 shows the effect of the nanoparticles volume fraction on the thermophoresis and buoyancy ratio parameters when $\varepsilon = 0.5$, $\Delta T = 20$, and $T_\infty = 30$ (the case of cone with a hot surface). Table 3 demonstrates that the increase of nanoparticles volume fraction decreases the buoyancy ratio parameter whereas it increases the thermophoresis parameter.

In the study of external natural convection of nanofluids, the investigation of the following three quantities: velocity, gradient of temperature and the gradient of nanoparticles concentration at the surface is very important. Therefore, Figs. 7–9 have been plotted to show the influence of the nanoparticles volume fraction and the nanoparticles size on the velocity, gradient of temperature and the gradient of nanoparticles concentration at the surface, respectively when the surface of the cone is hot.

Table 3
The variation of *Nr* and *Nt* for various values of nanoparticles volume fraction when $\varepsilon = 0.5$, $\Delta T = 20$, $T_\infty = 30$.

ϕ_∞	*Nt*	*Nr*
0.01	4.89E−06	696.302
0.02	9.63E−06	683.615
0.03	1.43E−05	671.761
0.04	1.90E−05	660.677
0.05	2.36E−05	650.308

By increasing the nanoparticles size and the nanoparticles volume fraction, the results that the velocity, $S'(0)$, and the gradient of nanoparticles concentration, $f'(0)$, at the surface of the cone raise whereas the temperature gradient profile decreases. The effects of d_p and ϕ_∞ on $S'(0)$ and $f'(0)$ are significant; however, these effects on $\theta'(0)$ are negligible (the variation of $\theta'(0)$ is in the order of 10^{-3}). As seen earlier, the effect of the nanoparticles concentration difference (comparison between the static and the dynamic models) on the thermo-physical properties is very low. Augmentation of d_p or ϕ_∞ increases the concentration difference at the surface ($\Delta\phi$). Hence, the absence of high density nanoparticles (because of concentration difference at the surface) leads to an increase of the surface velocity $S'(0)$ (see Fig. 7). Fig. 8 shows a very smooth decreasing trend of the surface temperature gradient, $\theta'(0)$ as a result of increasing the nanoparticles size and the nanoparticles volume fraction. However, the observed variation of the temperature gradient duo to increasing both d_p and ϕ_∞ is not significant.

Fig. 9 depicts that the augmentation of the ambient volume fraction and the nanoparticles size raises the nanoparticles concentration gradient, $f'(0)$, at the hot surface of the cone. The reason for this behavior is that the augmentation of d_p reduces the Brownian motion parameter as observed in Fig. 5. As already shown, the effect of variation of ϕ_∞ on the Brownian motion parameter is not significant. However, the increase of ϕ_∞ increases the thermophoresis parameter (*Nt*), and therefore, the nanoparticles concentration gradient at the cone surface increases.

In the previous research investigations [7–12], which have adopted the non-homogenous models, no effort was made to conduct a comparison between the convective heat transfer of the nanofluid and the base fluid. As presented in Section 2, a new relation, Eq. (22), was derived to perform this comparison. As discussed, this relation represents the ratio of the convective heat transfer of nanofluids to the convective heat transfer of the base fluid. Fig. 10a and b demonstrate the effects of the nanoparticles volume fraction and the nanoparticles size on the heat transfer ratio (h_{nf}/h_f) for the cases of the cone with a hot surface and a cold surface, respectively. Fig. 10a depicts that the heat transfer ratio is an increasing (or decreasing) function of the nanoparticles size (or nanoparticles volume fraction). In addition, the results reveal that the enhancement ratio, h_{nf}/h_f, is lower than unity in all cases. Therefore, dispersing nanoparticles in the cold base fluid does not enhance the convective heat transfer of the resulting nanofluid. Fig. 10b shows that the enhancement ratio is higher than unity for

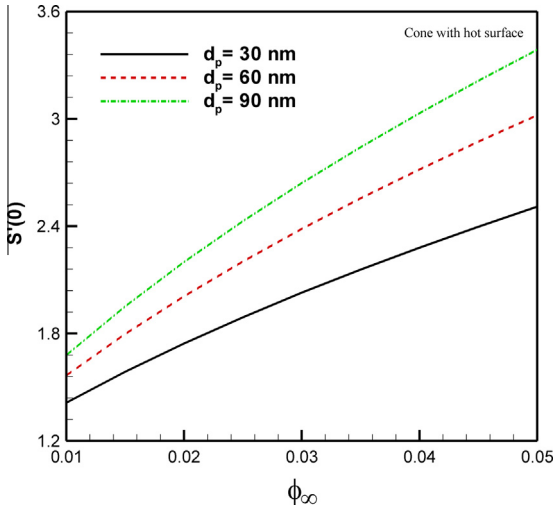

Fig. 7. The effects of nanoparticles volume fraction and diameter on the velocity, $S'(0)$.

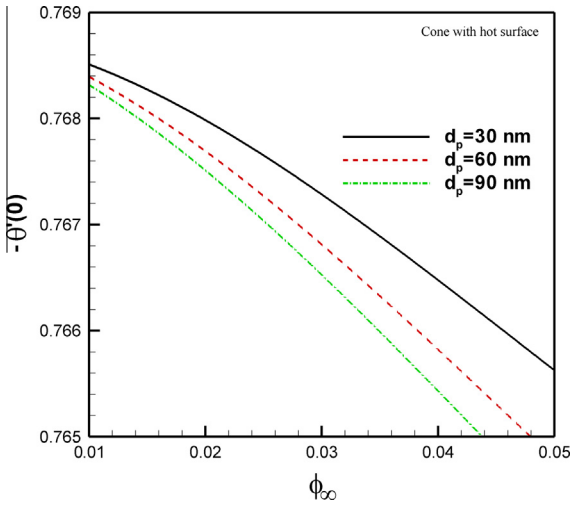

Fig. 8. The effects of nanoparticles volume fraction and diameter on the temperature gradient; $\theta'(0)$.

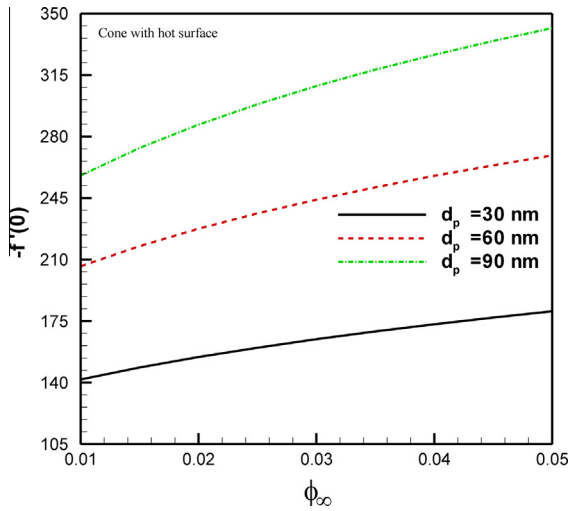

Fig. 9. The effects of nanoparticles volume fraction and diameter on the nanoparticles concentration gradient; $f'(0)$.

the case of cone with a cold surface. The results of this figure are in contrast with Fig. 10a. The migration of heavy nanoparticles into the surface increases the volume fractions of nanoparticles at the surface. The variation of thermo-physical properties of the nanofluid as a function of temperature affects the enhancement ratio. In addition, the presence of the heavy nanoparticles at the surface increases the buoyancy force because of the mass transfer. Furthermore, the increase of the volume fraction of nanoparticles at the surface results in the extra enhancement of the thermal conductivity (the higher volume fraction of nanoparticles, the higher thermal conductivity). Therefore, the enhancement of heat transfer can be seen in the case of cone with a cold surface.

In order to compare the convective heat transfer coefficients, i.e. $h_{Dynamic}$ and h_{Static}, evaluated using the dynamic and the static models, the enhancement ratio, Eq. (23), was introduced. Fig. 11 shows the variation of $h_{Dynamic}/h_{Static}$ as a function of the ambient nanoparticles volume fraction, ϕ_∞, and the size of nanoparticles, d_p when the cone surface is hot. The results depict that the difference between the heat transfer from the cone surface evaluated using the dynamic model and the static model is about 0.5%. Therefore, it can be concluded that there is no significant difference between

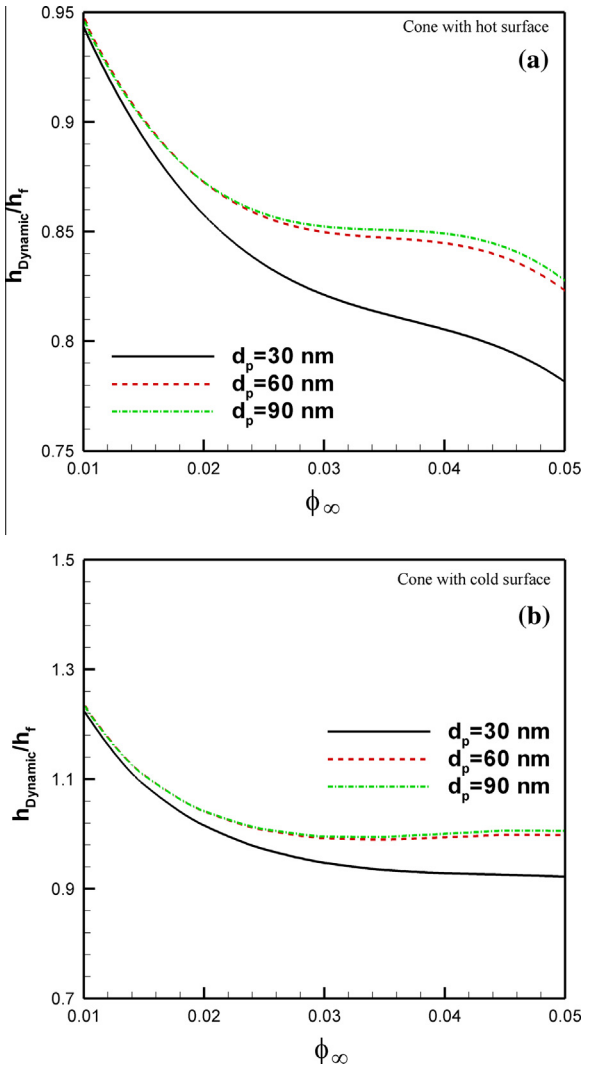

Fig. 10. The effects of nanoparticles volume fraction and diameter on the enhancement ratio, h_{nf}/h_f ((a) the cone with hot surface and (b) the cone with cold surface).

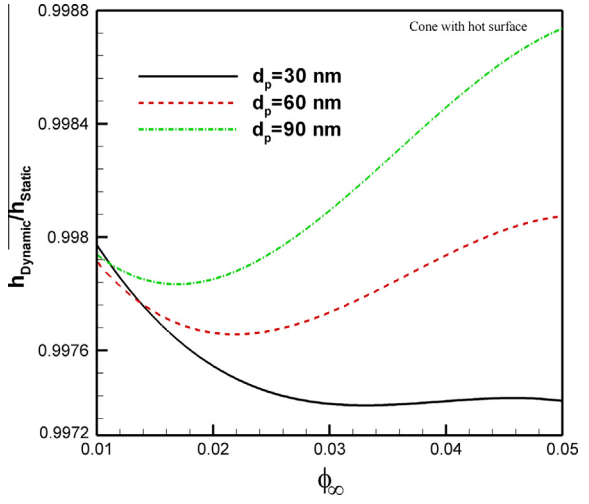

Fig. 11. The effects of nanoparticles volume fraction and diameter on the enhancement ratio, $h_{Dynamic}/h_{Static}$.

the results obtained using the dynamic model and those using the static model. In addition, by decreasing both the size and the volume fraction of nanoparticles, the dynamic model approaches the static model.

5. Important outcomes and conclusion

In this paper, a case study was performed to theoretically examine the natural convection heat transfer enhancement of Al_2O_3–water nanofluid around a vertical cone placed in a saturated porous medium. A new practical boundary condition, zero flux of nanoparticles at the cone surface is utilized. Moreover, the effects of the local temperature and the local volume fraction of nanoparticles are taken into account. The partial differential equations are reduced into a set of highly non-liner ordinary differential equations. The system of ordinary differential equations is a general function of the local thermal conductivity and the local dynamic viscosity. Thus, the governing equations can be solved for any arbitrary function of the thermal conductivity and the dynamic viscosity. Practical correlations obtained using regression on the available experimental data are employed to evaluate the dynamic viscosity and the thermal conductivity of nanofluids. The important outcomes of the present study can be summarized as follows:

(I) An augmentation of the nanoparticles size and the nanoparticles volume fraction raises the concentration difference, the non-dimensional nanoparticles concentration gradient and the non-dimensional velocity at the cone surface but reduces the non-dimensional temperature gradient at the cone surface for the case of a cone with a hot surface.

(II) For the case of a cone with a hot surface, the increase (or decrease) of the nanoparticles volume fraction (or nanoparticles size) tends to decrease the enhancement ratio. As one of the most important findings, the results reveal that the values of the enhancement ratio between the nanofluid and the base fluid, h_{nf}/h_f are less than unity which means that using nanoparticles in a base fluid cannot be helpful for increasing the natural convection heat transfer from the cone surface.

(III) For the case of a cone with a cold surface, the presence of nanoparticles enhances the heat transfer rate from the surface. Therefore, utilizing nanofluids in this case is helpful.

(IV) The enhancement ratio $h_{Dynamic}/h_{Static}$ has been derived to calculate the difference between the heat transfer coefficients obtained using the dynamic and the static models. The results depict that the value of this ratio is about unity. Therefore, the difference between the dynamic and the static models is negligible when the cone surface is hot. Moreover, in the case of a cone with a hot surface, the minimum and maximum values of the enhancement ratio ($h_{Dynamic}/h_{Static}$) are found to be about 0.9973 and 0.9987, respectively. Hence, for convenience, the dynamic effects of the Brownian motion and the thermophoresis causing the concentration gradient can be eliminated in the engineering applications.

Acknowledgement

The first author is grateful to Dezful Branch, Islamic Azad University for its support.

Appendix A

Substituting the stream function in the momentum equation in the direct of x-axis leads to:

$$\mu_{nf,\infty}\frac{1}{\kappa}\frac{\mu(\phi,T)}{\mu_{nf,\infty}}\frac{1}{r}\frac{\partial\psi}{\partial y}=\left[-\frac{\partial p}{\partial x}+(1-\phi_\infty)g\beta\rho_{f_\infty}\cos\gamma(T-T_\infty)-g\left(\rho_P-\rho_{f,\infty}\right)\cos\gamma(\phi-\phi_\infty)\right] \tag{A.1}$$

Differentiating Eq. (A.1) with respect to y, and differentiating the momentum equation in the direct of y-axis respect to x; then subtracting the equations to eliminate the pressure yields:

$$\frac{\mu_{nf,\infty}}{\kappa}\left(\frac{\mu(\phi,T)}{\mu_{nf,\infty}}\frac{1}{r}\frac{\partial^2\psi}{\partial y^2}+\frac{1}{\mu_{nf,\infty}}\frac{\partial\mu(\phi,T)}{\partial y}\frac{1}{r}\frac{\partial\psi}{\partial y}\right)=\left[(1-\phi_\infty)\beta g\rho_{f_\infty}\cos\gamma\left(\frac{\partial T}{\partial y}\right)-\left(\rho_P-\rho_{f_\infty}\right)g\cos\gamma\left(\frac{\partial\phi}{\partial y}\right)\right] \tag{A.2}$$

Using the similarity variables, each term in Eq. (A.2) is obtained as follows:

$$\frac{\partial\eta}{\partial y}=\frac{Ra_x^{\frac{1}{2}}}{x} \tag{A.3}$$

$$\frac{\partial\psi}{\partial S}=\alpha_{eff,nf}\cdot r\cdot Ra_x^{\frac{1}{2}} \tag{A.4}$$

$$\frac{\partial\psi}{\partial y}=\frac{\partial\psi}{\partial S}\frac{\partial S}{\partial\eta}\frac{\partial\eta}{\partial y}=\alpha_{eff,nf}\cdot r\cdot\frac{Ra_x}{x}S' \tag{A.5}$$

$$\frac{\partial^2\psi}{\partial y^2}=\left(\alpha_{eff,nf}\cdot r\cdot\frac{Ra_x^{\frac{3}{2}}}{x^2}\right)S'' \tag{A.6}$$

$$\frac{\partial\phi}{\partial y}=\frac{\partial\phi}{\partial f}\frac{\partial f}{\partial\eta}\frac{\partial\eta}{\partial y}=(\phi_w-\phi_\infty)\frac{Ra_x^{\frac{1}{2}}}{x}f' \tag{A.7}$$

$$\frac{\partial T}{\partial y}=\frac{\partial T}{\partial\theta}\frac{\partial\theta}{\partial\eta}\frac{\partial\eta}{\partial y}=(T_w-T_\infty)\left(\frac{Ra_x^{\frac{1}{2}}}{x}\right)\theta' \tag{A.8}$$

$$\frac{\partial\mu_{nf}(\phi,T)}{\partial y}=\left(\frac{\partial\mu_{nf}}{\partial f}\frac{\partial f}{\partial\eta}+\frac{\partial\mu_{nf}}{\partial\theta}\frac{\partial\theta}{\partial\eta}\right)\frac{\partial\eta}{\partial y}=\mu'_{nf}\frac{\partial\eta}{\partial y} \tag{A.9}$$

Substituting Eqs. (A.5), (A.7), and (A.8) into Eq. (A.2) yields to the following equation:

$$\frac{\mu_{nf,\infty}}{\kappa}\left(\frac{\mu_{nf}(f,\theta)}{\mu_{nf,\infty}}\frac{1}{r}\left(\alpha_{eff,nf}\cdot r\cdot\frac{Ra_x^{\frac{3}{2}}}{x^2}\right)S''+\frac{1}{\mu_{nf,\infty}}\left(\mu'_{nf}\frac{Ra_x^{\frac{1}{2}}}{x}\right)\frac{1}{r}\left(\alpha_{eff,nf}\cdot r\cdot\frac{Ra_x}{x}S'\right)\right)=\left[(1-\phi_\infty)\beta g\rho_{f_\infty}(T_w-T_\infty)\cos\gamma\left(\frac{Ra_x^{\frac{1}{2}}}{x}\right)\theta'-\left(\rho_P-\rho_{f_\infty}\right)g(\phi_w-\phi_\infty)\cos\gamma\frac{Ra_x^{\frac{1}{2}}}{x}f'\right] \tag{A.10}$$

where it can be simplified as:

$$\frac{\mu_{nf}(f,\theta)}{\mu_{nf,\infty}}S'+\left(\frac{\mu_{nf}(f,\theta)}{\mu_{nf,\infty}}\right)'S'-\theta'+\Delta\phi\times Nr\cdot f'=0 \tag{A.11}$$

where $Nr=\left(\rho_p-\rho_{f\infty}\right)/\left(\rho_{f\infty}\beta(T_w-T_\infty)(1-\phi_\infty)\right)$.

Now, using the similarity variables, each term of the heat equation, Eq. (13), is obtained as follows:

$$\frac{\partial^2 T}{\partial y^2}=(T_w-T_\infty)\left(\frac{Ra_x}{x^2}\right)\theta'' \tag{A.12}$$

$$\frac{\partial\phi^2}{\partial y^2}=(\phi_w-\phi_\infty)\left(\frac{Ra_x}{x^2}\right)f'' \tag{A.13}$$

$$\frac{\partial\eta}{\partial x}=\left(\frac{-1}{2}\right)y\frac{Ra_x^{\frac{1}{2}}}{x^2} \tag{A.14}$$

$$\frac{\partial \psi}{\partial x} = r\cdot S\cdot \frac{\partial}{\partial x}\left(\alpha_m Ra_x^{\frac{1}{2}}\right) + \left(\alpha_m\cdot r\cdot Ra_x^{\frac{1}{2}}\right)\cdot\frac{\partial S}{\partial \eta}\frac{\partial \eta}{\partial x} + \alpha_m Ra_x^{\frac{1}{2}} S\cdot\frac{\partial r}{\partial x}$$
$$= \frac{1}{2}\alpha_m r\frac{Ra_x^{\frac{1}{2}}}{x}S + \left(\alpha_m\cdot r\cdot Ra_x^{\frac{1}{2}}\right)\left(\frac{-1}{2}y\frac{Ra_x^{\frac{1}{2}}}{x^2}\right)S' + \alpha_m Ra_x^{\frac{1}{2}}\cdot\sin\gamma\cdot S$$
$$= \frac{1}{2}\alpha_m r\frac{Ra_x^{\frac{1}{2}}}{x}S - \frac{1}{2}\alpha_m\cdot r\cdot y\frac{Ra_x}{x^2}S' + \alpha_m Ra_x^{\frac{1}{2}}\cdot\sin\gamma\cdot S \quad (A.15)$$

$$\frac{\partial T}{\partial x} = \frac{\partial T}{\partial \theta}\frac{\partial \theta}{\partial \eta}\frac{\partial \eta}{\partial x} = (T_w - T_\infty)\left(\left(\frac{-1}{2}\right)y\frac{Ra_x^{\frac{1}{2}}}{x^2}\right)\theta' \quad (A.16)$$

$$\frac{\partial \phi}{\partial x} = \frac{\partial \phi}{\partial f}\frac{\partial f}{\partial \eta}\frac{\partial \eta}{\partial x} = (\phi_w - \phi_\infty)\left(\frac{-1}{2}y\frac{Ra_x^{\frac{1}{2}}}{x^2}\right)f' \quad (A.17)$$

$$\frac{\partial k_{nf}(\phi,T)}{\partial y} = \left(\frac{\partial k_{nf}}{\partial f}\frac{\partial f}{\partial \eta} + \frac{\partial k_{nf}}{\partial \theta}\frac{\partial \theta}{\partial \eta}\right)\frac{\partial \eta}{\partial y} = k'_{nf}\frac{\partial \eta}{\partial y} \quad (A.18)$$

Substituting Eqs. (A.5), (A.7), (A.8), and (A.12)–(A.18) into Eq. (13) yields:

$$(\rho c)_{nf}\left(\begin{array}{l}\frac{1}{r}\left(\alpha_{eff,nf,\infty}\cdot r\cdot\frac{Ra_x}{x}S'\right)(T_w - T_\infty)\left(\left(\frac{-1}{2}\right)y\frac{Ra_x^{\frac{1}{2}}}{x^2}\right)\theta' \\ -\frac{1}{r}\left(\frac{1}{2}\alpha_{eff,nf,\infty}\cdot r\cdot\frac{Ra_x^{\frac{1}{2}}}{x}S - \frac{1}{2}\alpha_{eff,nf,\infty}\cdot r\cdot y\frac{Ra_x}{x^2}S' + \alpha_{eff,nf,\infty}\sin\lambda\cdot Ra_x^{\frac{1}{2}}S\right)(T_w - T_\infty)\left(\frac{Ra_x^{\frac{1}{2}}}{x}\right)\theta'\end{array}\right)$$
$$= k_{m,\infty}k(f,\theta)(T_w - T_\infty)\left(\frac{Ra_x}{x^2}\right)\theta'' + k_{m,\infty}k'(f,\theta)\frac{Ra_x^{\frac{1}{2}}}{x}\left((T_w - T_\infty)\left(\frac{Ra_x^{\frac{1}{2}}}{x}\right)\theta'\right)$$
$$+\varepsilon(\rho c)_p\left[D_B(\phi_w - \phi_\infty)\frac{Ra_x^{\frac{1}{2}}}{x}f'(T_w - T_\infty)\left(\frac{Ra_x^{\frac{1}{2}}}{x}\right)\theta' + \left(\frac{D_T}{T_\infty}\right)\left((T_w - T_\infty)\left(\frac{Ra_x^{\frac{1}{2}}}{x}\right)\theta'\right)^2\right] \quad (A.19)$$

Eq. (A.19) can be simplified as:

$$\frac{k_{eff,nf}(f,\theta)}{k_{eff,nf,\infty}}\theta'' + \left(\frac{k_{eff,nf}(f,\theta)}{k_{eff,nf,\infty}}\right)'\theta' + \frac{3}{2}S\theta' + \Delta\phi\cdot Nb\cdot f'\theta' + Nt\cdot\theta' 2 = 0 \quad (A.20)$$

where $Nb = \frac{\varepsilon(\rho c)_p D_B}{(\rho c)_f \alpha_{eff,nf,\infty}}$ and $Nt = \frac{\varepsilon(\rho c)_p D_T (T_w - T_\infty)}{(\rho c)_f \alpha_m T_\infty}$.

Using the similarity variables, the two terms of Eq. (15) are written as:

$$\frac{\partial^2 \phi}{\partial y^2} = (\phi_w - \phi_\infty)\frac{Ra_x}{x^2}f'' \quad (A.21)$$

$$\frac{\partial \phi}{\partial x} = \frac{\partial \phi}{\partial f}\frac{\partial f}{\partial \eta}\frac{\partial \eta}{\partial x} = (\phi_w - \phi_\infty)\left(\frac{-1}{2}y\frac{Ra_x^{\frac{1}{2}}}{x^2}\right)f' \quad (A.22)$$

Substituting Eqs. (A.5), (A.7), (A.12), (A.21) and (A.22) into the conservation of the nanoparticles, Eq. (15) leads to the following equation:

$$\frac{1}{\varepsilon}\left[\frac{1}{r}\times\left(\alpha_{eff,nf,\infty}\cdot r\cdot\frac{Ra_x}{x}S'\right)\times\left((\phi_w - \phi_\infty)\left(\frac{-1}{2}y\frac{Ra_x^{\frac{1}{2}}}{x^2}\right)f'\right)\right.$$
$$-\frac{1}{r}\times\left(\frac{1}{2}\alpha_{eff,nf,\infty}\cdot r\cdot\frac{Ra_x^{\frac{1}{2}}}{x}S + \left(\alpha_{eff,nf,\infty}\cdot r\cdot Ra_x^{\frac{1}{2}}\right)\left(\frac{-1}{2}y\frac{Ra_x^{\frac{1}{2}}}{x^2}\right)S'\right.$$
$$\left.\left.+\alpha_{eff,nf,\infty}\sin\gamma\cdot Ra_x^{\frac{1}{2}}\cdot S\right)\times(\phi_w - \phi_\infty)\frac{Ra_x^{\frac{1}{2}}}{x}f'\right]$$
$$= D_B\left((\phi_w - \phi_\infty)\frac{Ra_x}{x^2}f''\right) + \frac{D_T}{T_\infty}\left((T_w - T_\infty)\left(\frac{Ra_x}{x^2}\right)\theta''\right) \quad (A.23)$$

Eq. (A.23) can be simplified as:

$$f'' + \frac{3}{2}Le\cdot Sf' + \frac{Nt}{\Delta\phi\cdot Nb}\theta'' = 0 \quad (A.24)$$

where $\frac{Nt}{Nb} = \frac{D_T(T_w - T_\infty)}{T_\infty D_B}$ and $Le = \frac{\alpha_{eff,nf,\infty}}{\varepsilon D_B}$ (A.25)

Appendix B

Using the standard reference data, the thermal conductivity of water is computed from the following relation [22]

$$k_f = 0.6065\times\left(-1.48445 + 4.12292\frac{T}{298.15} - 1.63866\left(\frac{T}{298.15}\right)^2\right)$$
$$\times\ \text{for}\ 274\leqslant T\leqslant 370 \quad (B.1)$$

where k_f is the thermal conductivity of water and T is the absolute temperature.

The first derivatives of μ and $k_{eff,nf}$ are needed for the solution of Eqs. (12)–(14), these terms, using Eqs. (8)–(10), are obtained as follows:

For the dynamic viscosity of nanofluid:

$$\mu_{nf}(f,\theta) = \left(\begin{array}{l}-0.4491 + \frac{28.837}{T} + 0.574\phi\times 10^2 - 0.1634\phi^2\times 10^4 + 23.053\frac{\phi^2}{T^2}\times 10^4 \\ +0.0132\phi^3\times 10^6 - 2354.735\frac{\phi}{T^3}\times 10^2 + 23.498\frac{\phi^2}{d_p^2}\times 10^4 - 3.0185\frac{\phi^3}{d_p^2}\times 10^6\end{array}\right)\times 10^{-3}$$
$$0.01\leqslant\phi\leqslant 0.09,\quad 20\leqslant T(^\circ\mathrm{C})\leqslant 70,\quad 13\,\mathrm{nm}\leqslant d_p\leqslant 131\,\mathrm{nm}$$

$$\frac{d\mu_{nf}(f,\theta)}{d\eta} = \theta'\times\Delta T\times 10^{-3}\left(-\frac{28.837}{(\theta\cdot\Delta T + T_\infty)^2} - 46.106\frac{(f\Delta\phi + \phi_\infty)^2}{(\theta\cdot\Delta T + T_\infty)^3}\times 10^4 + 7064.205\frac{(f\Delta\phi + \phi_\infty)}{(\theta\cdot\Delta T + T_\infty)^4}\times 10^2\right)$$
$$+f'\times\Delta\phi\times 10^{-3}\left(\begin{array}{l}0.574\times 10^2 - 0.3268(f\Delta\phi + \phi_\infty)\times 10^4 + 46.106\frac{(f\Delta\phi + \phi_\infty)}{(\theta\cdot\Delta T + T_\infty)^2}\times 10^4 + 0.0396(f\Delta\phi + \phi_\infty)^2\times 10^6 \\ -2354.735\frac{1}{(\theta\cdot\Delta T + T_\infty)^3}\times 10^2 + 46.996\frac{(f\Delta\phi + \phi_\infty)}{dp^2}\times 10^4 - 9.0555\frac{(f\Delta\phi + \phi_\infty)^2}{dp^2}\times 10^6\end{array}\right) \quad (B.2)$$

For the effective thermal conductivity of the porous medium and the nanofluid:

$$\frac{dk_{eff,nf}(f,\theta)}{d\eta} = \varepsilon k_s^{1-\varepsilon} k_{nf}^{\varepsilon-1} \frac{dk_{nf}(f,\theta)}{d\eta} \tag{B.3}$$

where

$$k_{nf} = k_f \begin{pmatrix} 0.9843 + 0.398\left(\phi \times 10^2\right)^{0.7383} d_p^{-0.2246} \left(\frac{\mu_{nf}}{\mu_f}\right)^{0.0235} \\ -3.9517\frac{\phi}{T} \times 10^2 + 34.034\frac{\phi^2}{T^3} \times 10^4 + 32.509\frac{\phi}{T^2} \times 10^2 \end{pmatrix}$$

$$0.0 \leqslant \phi \leqslant 0.10, \quad 20 \leqslant T(^\circ\mathrm{C}) \leqslant 70, \quad 11\ \mathrm{nm} \leqslant d_p \leqslant 150\ \mathrm{nm}$$

$$\frac{dk_{nf}(f,\theta)}{d\eta} = \theta' \times \Delta T \times k_f \begin{pmatrix} 3.9517\frac{(f\Delta\phi+\phi_\infty)}{(\theta\cdot\Delta T+T_\infty)^2} \times 10^2 - 102.102\frac{(f\Delta\phi+\phi_\infty)^2}{(\theta\cdot\Delta T+T_\infty)^4} \times 10^4 \\ -65.018\frac{(f\Delta\phi+\phi_\infty)}{(\theta\cdot\Delta T+T_\infty)^3} \times 10^2 \end{pmatrix}$$

$$+ \theta' \times \Delta T \times k_f \left(0.398 \times 0.0235 \times 10^{1.4766} \times (f\Delta\phi+\phi_\infty)^{0.7383} \times \frac{1}{dp^{0.2246}} \left(\frac{\mu_{nf}}{\mu_f}\right)^{-0.9765} \frac{\mu_f \frac{d\mu_{nf}}{d\eta} - \mu_{nf}\frac{d\mu_f}{d\eta}}{\mu_f^2}\right) \tag{B.4}$$

$$f' \times \Delta\phi \times k_f \begin{pmatrix} 0.2938\frac{1}{(f\Delta\phi+\phi_\infty)^{0.2617} dp^{0.2246}} \times \left(\frac{\mu_{nf}}{\mu_f}\right)^{0.0235} \times 10^{1.4766} - 3.9517\frac{1}{(\theta\cdot\Delta T+T_\infty)} \times 10^2 \\ +68.068\frac{(f\Delta\phi+\phi_\infty)}{(\theta\cdot\Delta T+T_\infty)^3} \times 10^4 + 32.509\frac{1}{(\theta\cdot\Delta T+T_\infty)^2} \times 10^2 \end{pmatrix}$$

and

$$\frac{d\mu_f}{d\eta} = -5.981892 \times 10^{-5} \times 10^{\frac{247.8}{(\theta\Delta T+T_\infty)+133}} \times \frac{\ln(10)}{(\theta\Delta T+T_\infty+133)^2} \Delta T \times \theta' \tag{B.5}$$

The density (ρ_{nf}) of the nanofluid is evaluated using the following relation [15]:

$$\rho_{nf} = (1-\phi_\infty)\rho_f + \phi_\infty \rho_p \tag{B.6}$$

where ρ_f and ρ_p denote the density of the base fluid and the nanoparticles, respectively. The heat capacity of nanofluid $(\rho c)_{nf}$ is also obtained as follows [15]:

$$(\rho c)_{nf} = (1-\phi_\infty)(\rho c)_f + \phi_\infty (\rho c)_p \tag{B.7}$$

where $(\rho c)_f$ and $(\rho c)_p$ denote the heat capacity of the base fluid and the heat capacity of the nanoparticles, respectively. The Brownian motion coefficient D_B is obtained using the following relation [3]:

$$D_B = \frac{k_B T_\infty}{3\pi\mu_{f,\infty} d_p} \tag{B.8}$$

where $\mu_{f,\infty}$ (Pa s) is the dynamic viscosity of the base fluid, T_∞ (K) is the absolute temperature of the ambient free stream. d_p (m) is the diameter of the nanoparticles and $k_B = 1.3807 \times 10^{-23}$ (J/K) is the Boltzmann's constant. The thermophoresis coefficient D_T is evaluated using the following relation [3]:

$$D_T = 0.26\left(\frac{k_f}{2k_f+k_p}\right)\frac{\mu_{f,\infty}}{\rho_{f,\infty}}\phi_\infty \tag{B.9}$$

where k_f is the thermal conductivity of the base fluid and k_p is the thermal conductivity of the nanoparticles. $\mu_{f,\infty}$ and $\rho_{f,\infty}$ are the dynamic viscosity and the density of water, respectively.

References

[1] R.S.R. Gorla, A.J. Chamkha, A.M. Rashad, Mixed convective boundary layer flow over a vertical wedge embedded in a porous medium saturated with a nanofluid: Natural Convection Dominated Regime, Nanoscale Res. Lett. 6 (2011) 1–9.

[2] R. Saidur, K.Y. Leong, H.A. Mohammad, A review on applications and challenges of nanofluids, Renew. Sustain. Energy Rev. 15 (2011) 1646–1668.

[3] J. Buongiorno, Convective transport in nanofluids, J. Heat Transfer 128 (2006) 240–250.

[4] S.K. Das, S. Choi, W. Yu, T. Pradeep, Nanofluids: Science and Technology, John Wiley & Sons, New Jersey, 2007.

[5] D.A. Nield, A.V. Kuznetsov, The Cheng–Minkowycz problem for natural convective boundary-layer flow in a porous medium saturated by a nanofluid, Int. J. Heat Mass Transf. 52 (2009) 5792–5795.

[6] Yih, The effect of uniform lateral mass flux on free convection about a vertical cone embedded in a saturated porous media, Int. Commun. Heat Mass Transfer 24 (1997) 1195–1205.

[7] A.M. Rashad, M.A. El-Hakiem, M.M.M. Abdou, Natural convection boundary layer of a non-Newtonian fluid about a permeable vertical cone embedded in a porous medium saturated with a nanofluid, Comput. Math. Appl. 62 (2011) 3140–3151.

[8] R.S.R. Gorla, A.J. Chamkha, Natural convective boundary layer flow over a horizontal plate embedded in a porous medium saturated with a nanofluid, J. Mod. Phys. 2 (2011) 62–71.

[9] A. Chamkha, R.S.R. Gorla, K. Ghodeswar, Non-similar solution for natural convective boundary layer flow over a sphere embedded in a porous medium saturated with a nanofluid, Transp. Porous Media 86 (2010) 13–22.

[10] P. Rana, R. Bhargava, O.A. Bég, Numerical solution for mixed convection boundary layer flow of a nanofluid along an inclined plate embedded in a porous medium, Comput. Math. Appl. 64 (2012) 2816–2832.

[11] A. Noghrehabadi, A. Behseresht, M. Ghalambaz, J. Behseresht, Natural-convection flow of nanofluids over a vertical cone embedded in non-Darcy porous media, J. Thermophys. Heat Transfer 27 (2013) 334–341.

[12] A. Noghrehabadi, A. Behseresht, M. Ghalambaz, Natural convection of nanofluid over vertical plate embedded porous medium, Appl. Math. Mech. (English Edition) 34 (2013) 669–686.

[13] A. Noghrehabadi, A. Behseresht, Flow and heat transfer affected by variable properties of nanofluids in natural-convection over a vertical cone in porous media, Comput. Fluids 88 (2013) 313–325.

[14] R.S.R. Gorla, A. Chamkha, K. Ghodeswar, Natural convective boundary layer flow over a vertical cone embedded in a porous medium saturated with a nanofluid, J. Nanofluids 3 (2014) 65–71.

[15] K. Khanafer, K. Vafai, A critical synthesis of thermophysical characteristics of nanofluids, Int. J. Heat Mass Transf. 54 (2011) 4410–4428.

[16] M. Chandrasekar, S. Suresh, A review on the mechanisms of heat transport in nanofluids, Heat Transfer Eng. 30 (2009) 1136–1150.

[17] L.F. Shampine, J. Kierzenka, M.W. Reichelt, Solving boundary value problems for ordinary differential equations in MATLAB with bvp4c, Tutorial Notes, 2000.

[18] D.A. Nield, A. Bejan, Convection in Porous Media, fourth ed., Springer, New York, 2013.

[19] P. Cheng, T.T. Le, I. Pop, Natural convection of a Darcian fluid about a cone, Int. Commun. Heat Mass Transfer 12 (1985) 705–717.

[20] A. Behseresht, A. Noghrehabadi, M. Ghalambaz, Natural-Convection heat and mass transfer from a vertical cone in porous media filled with nanofluids using the practical ranges of nanofluids thermo-physical properties, Chem. Eng. Res. Des. 92 (2014) 447–452.

[22] H. Curtis, Orbital Mechanics for Engineering Students, Academic Press, 2009. Appendix D.4.

[22] M.L.V. Ramires, C.A. Nieto de Castro, Y. Nagasaka, A. Nagashima, M.J. Assael, W.A. Wakeham, Standard reference data for the thermal conductivity of water, J. Phys. Chem. Ref. Data 24 (1995) 1377.